Interface connections of a transmembrane voltage sensor

J. Alfredo Freites*, Douglas J. Tobias†, Gunnar von Heijne‡, and Stephen H. White*§

*Department of Physiology and Biophysics and Program in Macromolecular Structure, University of California, Irvine, CA 92697-4560; †Department of Chemistry and Institute for Surface and Interface Science, University of California, Irvine, CA 92697-2025; and ‡Department of Biochemistry and Biophysics, Stockholm University, SE-106 91 Stockholm, Sweden

Communicated by Roderick MacKinnon, The Rockefeller University, New York, NY, September 1, 2005 (received for review July 4, 2005)

Voltage-sensitive ion channels open and close in response to changes in transmembrane (TM) potential caused by the motion of the S4 voltage sensors. These sensors are α–helices that include four or more positively charged amino acids, most commonly arginine. The so-called paddle model, based on the high-resolution structure of the KvAP K^+ channel [Jiang, *et al.* (2003) *Nature* 423, 33–41], posits that the S4 sensors move within the membrane bilayer in response to TM voltage changes. Direct exposure of S4 sensors to lipid is contrary to the classical expectation that the dielectric contrast between the membrane hydrocarbon core and water presents an insurmountable energetic penalty to burial of electric charges. Nevertheless, recent experiments have shown that a helix with the sequence of KvAP S4 can be inserted across the endoplasmic reticulum membrane. To reconcile this result with the classical energetics argument, we have carried out a molecular dynamics simulation of an isolated TM S4 helix in a lipid bilayer. The simulation reveals a stabilizing hydrogen-bonded network of water and lipid phosphates around the arginines that reduces the effective thickness of the bilayer hydrocarbon core to ≈10 Å in the vicinity of the helix. It suggests that bilayer phospholipids can adapt locally to strongly perturbing protein elements, causing the phospholipids to become a structural extension of the protein.

voltage-gated potassium channels | lipid bilayer structure | membrane electrostatics | molecular dynamics simulation | membrane proteins

Voltage-sensitive ion channels (reviewed in ref. 1), which probably exist in all life forms (2), control the flow ionic currents down transmembrane (TM) electrochemical gradients in response to changes in membrane potential. They do this by opening and closing in response to changes in TM potential as a result of the motion of voltage-sensor domains (3). Voltage-gated potassium (Kv) channels, perhaps the most intensely studied family of voltage-sensitive channels, are typically homotetramers assembled from monomers that have six TM helices (S1–S6) with a pore domain between S5 and S6. The principal voltage-sensing component is the S4 helix. Although rich in hydrophobic residues, it includes four or more positively charged amino acids, most commonly arginine, that cause S4 to respond to changes in membrane potential.

The mechanistic details of the S4 response in Kv channels is a matter of considerable debate (4–8). The focus of the discussion is the so-called paddle model (9), which derives from the high-resolution structure (10) of the KvAP K^+ channel from the archaebacterium *Aeropyrum pernix* (11), and more recently the structure of a mammalian voltage-dependent K^+ channel (12, 13). This model posits that the four voltage paddles of the homotetramer, comprised of part of S3 (S3b) and S4, move within the membrane bilayer in response to TM voltage changes. The alternative view is that S4 moves inside water-filled canaliculi hidden from the bilayer by other parts of the channel protein (14). Although experimental studies show that synthetic peptides related to the S4 voltage sensor readily adopt surface-bound configurations with model membranes (15, 16), a TM configuration is contrary to the classical expectation that the dielectric contrast between the membrane hydrocarbon core and water presents an insurmountable energetic penalty to burial of electric charges (17, 18).

A key question is thus whether an isolated S4 segment can exist as a TM helix in the absence of the rest of the protein. This question was answered by Hessa *et al.* (19) by means of an experimental system that permits accurate measurements (20) of the apparent free energy (ΔG_{app}) of translocon-mediated integration of TM helices into the endoplasmic reticulum (ER) membrane. They found that a S4 model helix based on the KvAP voltage sensor (GGPG-LGLFRLVRLLRFLRILLII-GPGG) partitioned about equally between the membrane-inserted and noninserted (secreted) states during assembly by the translocon. Specifically, the S4 model could be inserted across the ER membrane with a ΔG_{app} of 0.5 kcal·mol^{-1}. A mutant of S4 (S4mut), in which two of four arginines were moved one step toward the C terminus, inserted even better (ΔG_{app} = 0.0 kcal·mol^{-1}). We consider in this article the question of how it is possible for the S4 model helix to be inserted across the ER membrane. Although the structure and location of the noninserted population of S4 is unknown, it might be surface-bound as observed in model membrane systems (15, 16). But in any case, we consider here only the physical basis for the TM-inserted state.

Two explanations for the Hessa *et al.* (19) result are possible. One is that an inserted S4 helix associates with some other ER protein, thus shielding it from the lipid bilayer by salt-bridge formation or some kind of canaliculi. The other explanation is that the S4-model helix is fully exposed to lipid. This explanation is more likely. In a thorough examination of the translocon-assisted insertion of model helices across the ER membrane, Hessa *et al.* (20) determined a biological hydrophobicity scale based on measurements of ΔG_{app} for a large number of 19-aa-long test segments (H segments) flanked on the N and C termini by GGPG–and –GPGG, respectively. The resulting base hydrophobicity scale provided values of ΔG^{app}_{AA} for each of the natural amino acids in the center position of the H segment. They discovered, however, that the ΔG^{app}_{AA} for tyrosine, tryptophan, and charged residues depended strongly on position within the H segment. The values of ΔG^{app}_{AA} were unfavorable in the center position, but became much less so as the residues were moved toward either of the H-segment ends. From the base biological scale and measurements of the position dependence of ΔG^{app}_{Arg} and ΔG^{app}_{Gly}, Hessa *et al.* (19) were able to compute with remarkable accuracy the ΔG_{app} values observed for S4 and S4mut. The close agreement of the computed and observed free energy values indicates that position-adjusted additivity prevails in the insertion of S4 and that shielding of S4 by other ER proteins need not be invoked to explain the observed values of ΔG_{app}.

Freely available online through the PNAS open access option.

Abbreviations: TM, transmembrane; Kv, voltage-gated potassium; ER, endoplasmic reticulum; MD, molecular dynamics; ΔG_{app}, apparent free energy.

§To whom correspondence should be addressed. E-mail: blanco@helium.biomol.uci.edu.

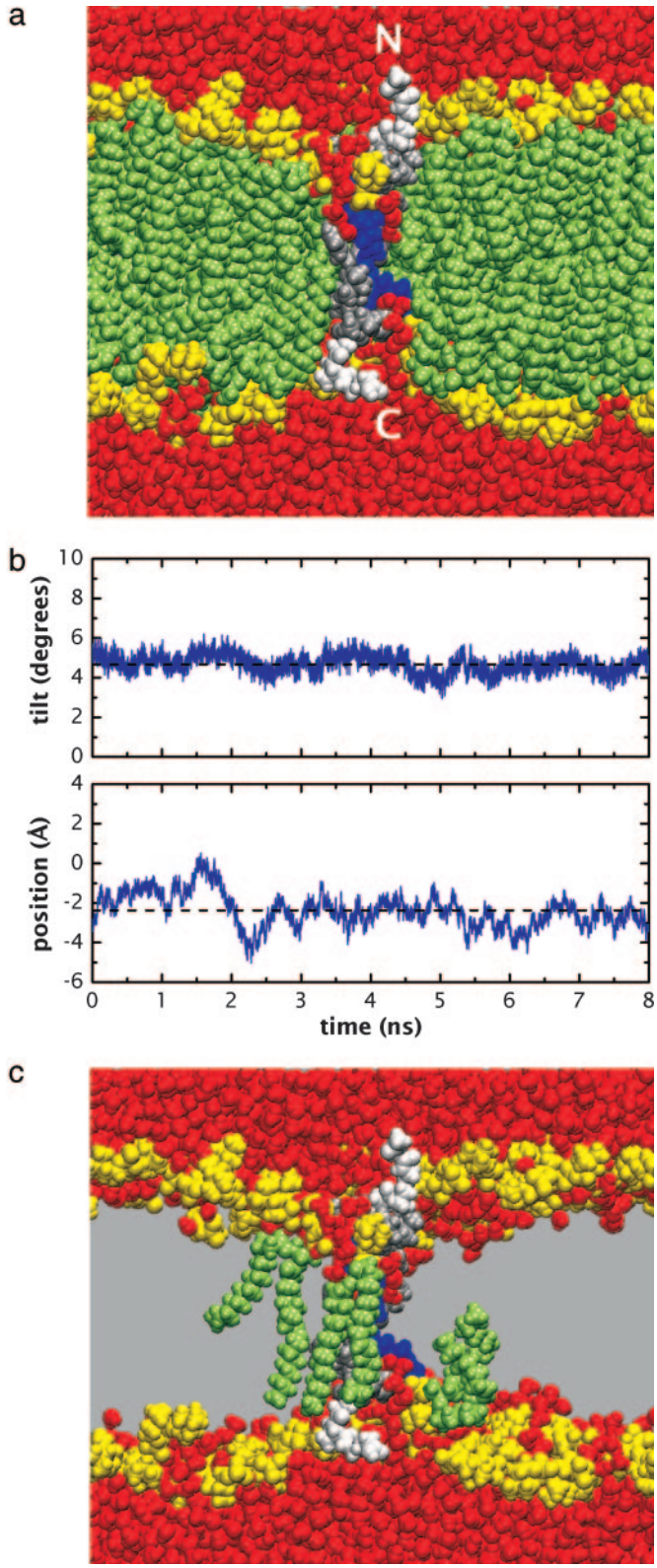

Fig. 1. MD simulation of a model S4 voltage-sensor peptide (GGPG-LGLFRLVRLLRFLRILLII-GPGG) in a palmitoyloleoylphosphatidylcholine bilayer. This model was chosen because it is the one studied by Hessa *et al.* (19). The simulation was carried out to understand the physical basis for the stable insertion of S4 across the ER by the translocon. (*a*) Cut-away view of the simulation system, showing the bilayer distortion around the peptide and the contacts between phosphate groups, water molecules, and arginine side chains. Red indicates water; yellow, phosphocholine headgroups; green, acyl chains; white, GGPG . . . GPGG flanks; silver, non-Arg S4 residues; blue, arginine side chains. (*b*) MD trajectories of the S4 helix tilt angle relative to the bilayer normal (*Upper*) and the S4 helix center of mass relative to the center of mass of the lipid bilayer (*Lower*). The average values of the tilt angle and center of mass are, respectively, 4.67 ± 0.47 (SD) degrees and −2.37 ± 0.85 (SD) Å. (*c*) The phospholipids in the vicinity of the S4 helix that form H bonds with the guanidinium groups (see Fig. 2). The system configuration is the same as in *a*, except that only the three lipids participating in the H bonds are shown. These three lipids formed a stable H-bonded complex with S4 that remained unbroken during the last 5 ns of the simulation (see Fig. 2*b*). One of the lipids spans the entire membrane, in a configuration akin to a lipid in a monolayer, underscoring the extreme distortion of the bilayer in the vicinity of S4.

To gain insights into how S4 can be inserted across a membrane, we have carried out a molecular dynamics (MD) simulation of an isolated S4 helix in a TM configuration across a lipid bilayer. Specifically, the S4-model helix used in the Hessa *et al.* (19) experiments, GGPG–LGLFRLVRLLRFLRILLII–GPGG, was inserted across a lipid bilayer comprised of palmitoyloleoylphosphatidylcholine. The simulation reveals a stabilizing hydrogen-bonded network of water and lipid phosphates around the arginines that reduces the effective thickness of the bilayer hydrocarbon core to ≈10 Å in the vicinity of the helix.

Methods

An all-atom model of the S4 peptide studied by Hessa *et al.* (19) was built with the software package CHARMM 2.3 (21). The model S4 segment (-LGLFRLVRLLRFLRILLII-) was assembled as an ideal α-helix, whereas the flanking residues (GGPG– . . . –GPGG) were assembled in an extended conformation. To relax the conformation of the flanks and eliminate bad contacts, the initial structure was submitted to three rounds of 5,000-step conjugate-gradient energy minimization, 50 ps of MD at 600 K, and 100 ps of MD at 300 K. During these runs, all hydrogen atoms were free to move, all of the nonhydrogen atoms of the S4 segment were fixed, and all of the nonhydrogen atoms of the flank residues were restrained by harmonic potentials, which were released progressively.

The relaxed-model peptide was then inserted into a previously equilibrated all-atom palmitoyloleoylphosphatidylcholine model bilayer with excess water. To perform the insertion, the centers of mass of the bilayer system and the peptide were made to coincide, the peptide's principal axis was aligned normal to the bilayer, and its final location was adjusted so that the four arginine residues of the S4 segment were positioned symmetrically with respect to the bilayer midplane. The lipid molecules from each bilayer leaflet that overlapped with the peptide were removed from the system. It was necessary to remove only three lipids from each leaflet. The final system was composed of the peptide, 268 lipid molecules, 12,107 water molecules, and 4 negative counterions, for a total of 72,683 atoms. The dimensions of the initial simulation cell were 96.0472 × 96.3806 × 74.7126 Å.

The initial system equilibration process consisted of 5,000 steps of energy minimization, followed by a series of 100-ps MD runs at constant volume and constant temperature (300 K). The first of these runs was carried out only over the lipid molecules that formed the first coordination shell of the peptide. This run was followed by a run over all of the waters and a run over lipids, waters, and counterions. The full simulation was then carried out at constant temperature of 300 K and constant pressure of 1 atm (1 atm = 101.3 kPa). The peptide was progressively released from its initial configuration over five 100-ps steps, each using harmonic restraints.

All of the MD runs were conducted with the NAMD 2.5 software package (22). The CHARMM22 and CHARMM27 force fields (23, 24) were used for the peptide and the lipids, respectively, and the TIP3P model was used for water (25). The smooth particle

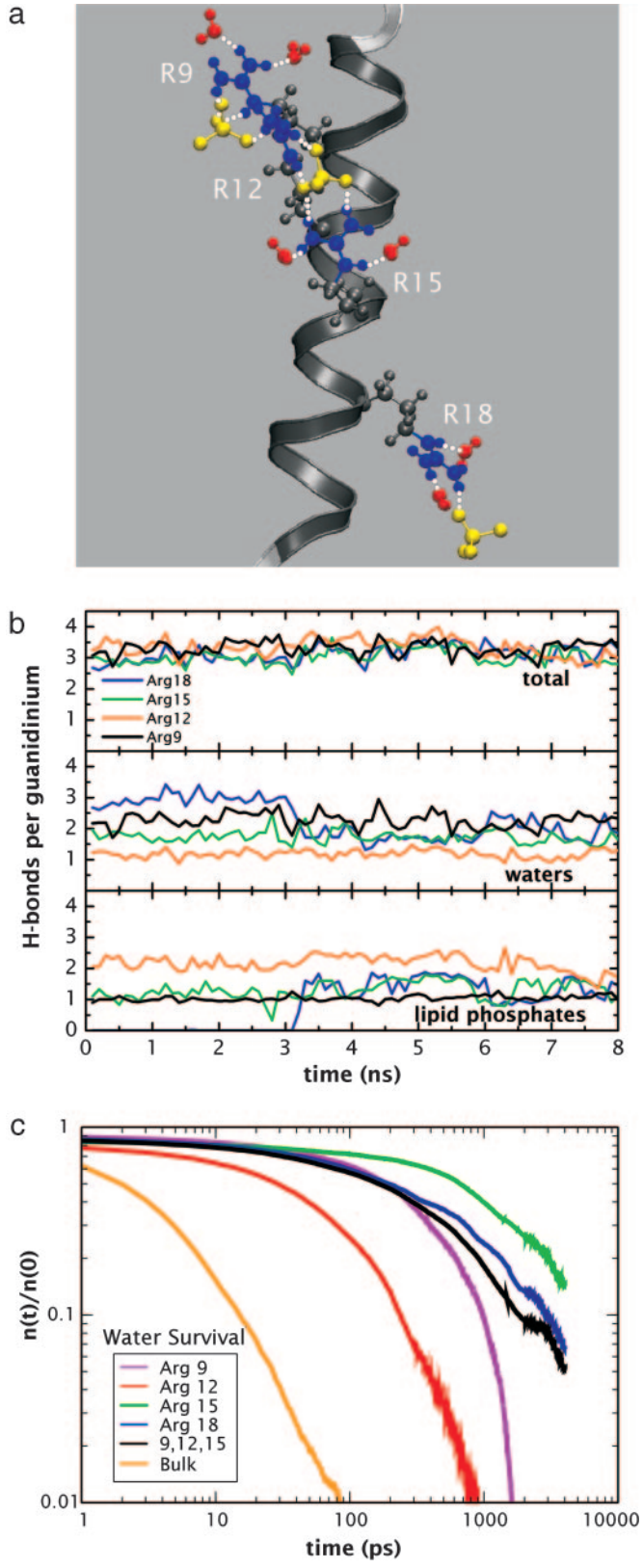

Fig. 2. Hydrophilic neighborhood of the S4 helix in the lipid bilayer. (*a*) Stabilizing hydrogen-bond network of water (red) and lipid phosphates (yellow) that connect the Arg guanidinium groups (blue) to the bilayer interface. H bonds are indicated by white dots. (*b*) MD trajectories of the number of hydrogen-bond contacts per guanidinium group. Total number of H bonds (*Top*), water H bonds (*Middle*), and lipid phosphate groups (*Bottom*). These data indicate that the H-bond capacities of the guanidinium groups are saturated throughout the simulation. (*c*) Survival functions for water molecules in the hydrophilic neighborhood of each Arg and in the equivalent volume of bulk water (see *Supporting Text*). A survival function calculation taking into account the overlap of coordination shells for Arg-9, Arg-12, and Arg-15 to form a single hydrophilic neighborhood is indicated by the black curve, which is remarkably similar to the survival function for Arg-18, consistent with the idea of two similar, but independent, solvation environments. From these data, the mean residence times for waters are found to be 364 ps for Arg-9, 92 ps for Arg-12, 2,172 ps for Arg-15, and 1,130 ps for Arg-18 compared with 6 ps for bulk water.

mesh Ewald method (26, 27) was used to calculate electrostatic interactions, and the short-range real-space interactions were cut off at 11 Å, by using a switching function. A reversible multiple time–step algorithm (28) was used to integrate the equations of motion with a time step of 4 fs for electrostatic forces, 2 fs for short-range nonbonded forces, and 1 fs for bonded forces. All bond lengths involving hydrogen atoms were held fixed by using the SHAKE algorithm. A Langevin dynamics scheme was used for thermostating. Nosé-Hoover-Langevin pistons were used for pressure control (29, 30). Molecular graphics and simulation analyses were generated with the VMD 1.8.3 software package (31). The electrostatic potential maps were obtained from the average of a particle mesh Ewald calculation over 800 configurations spanning the last 8 ns of the simulation by using the PMEPOT plug-in for VMD.

Results and Discussion

The S4 helix was simulated in a palmitoyloleoylphosphatidylcholine bilayer in excess water. Because the existence of a potential across the ER membrane is uncertain (32), no electric field was imposed across the membrane. The simulation was run for 16.5 ns (Fig. 1), but the analysis was performed only over the last 8 ns, after the system had reached a stationary state. Even though no conformational constraints of any kind were used, the S4 helix remained in a stable TM configuration throughout the simulation without any sign of the peptide drifting out of the bilayer. This lack of drift is demonstrated by the trajectory of its center of mass and tilt angle (Fig. 1*b*). One can therefore reasonably assume that the simulation was sampling configurations representative of the thermodynamically stable, inserted population of S4 in the ER translocon experiment. The organization of the bilayer was highly perturbed in the immediate vicinity of the S4 helix, as illustrated by the unusual conformations of the lipids whose headgroups interacted strongly with the S4 guanidiniums (Fig. 1*c*). These unusual conformations are not observed in simulations of purely hydrophobic TM helices, even very short ones with basic residues in the flanking regions (S. Jaud, G.v.H., D.J.T., and S.H.W., unpublished data).

Fig. 2*a* reveals the basis for TM helix stability. A hydrogen-bonded network of water and lipid phosphate groups formed around the guanidinium groups of the S4 arginines, as a result of local distortions of bilayer lipids close to the peptide (Fig. 1*c*). The H-bonding capacity of the four guanidinium groups was saturated throughout the equilibrated trajectory, as indicated by the participation of each guanidinium group in three H bonds with water and lipid phosphates (Fig. 2*b*). The H-bonded network creates two hydrophilic neighborhoods, one at each end of the helix, that connect the arginines to the hydrated bilayer interfaces. These neighborhoods consist in part of strings of water molecules that penetrate into the hydrocarbon core of the bilayer. Water penetration of this sort is not without precedent. A string of water molecules connecting a fully buried glutamate residue was observed in a high-resolution crystallographic structure of a mutant staphylococcal nuclease (33). The additional feature seen in the present case is the participation of the lipid phosphates, which apparently facilitate water penetration for

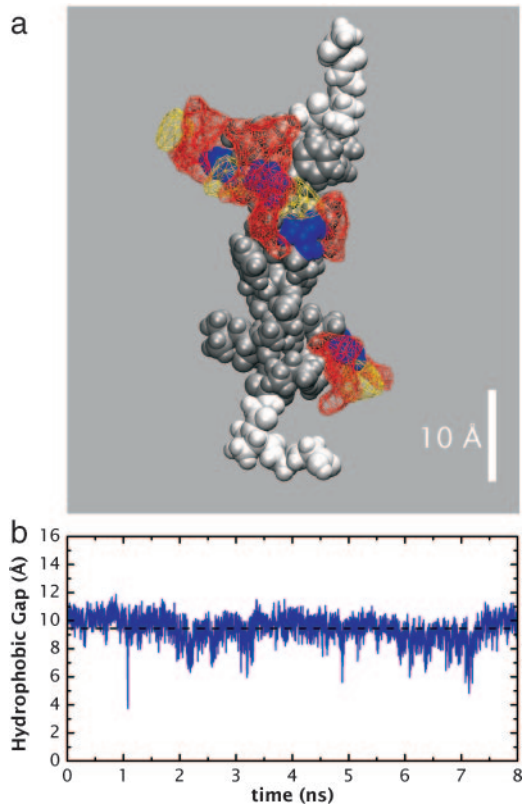

Fig. 3. Hydrophobic gap between Arg-15 and Arg-18. (*a*) Space-filling representation of the hydrophilic neighborhood of the S4 helix represented as Connolly surfaces. Red indicates water; yellow, phosphocholine headgroups; green, acyl chains; white, GGPG . . . GPGG flanks; silver, non-Arg S4 residues; blue, guanidinium groups. (*b*) MD trajectory of the hydrophobic gap, which is defined as the instantaneous distance parallel to the membrane normal, between any two H-bond forming atoms (nonhydrogens) on opposite sides of the bilayer center. The possible atoms are guanidinium nitrogens, water oxygens, and lipid phosphates. The average gap distance is 9.46 ± 0.86 (SD) Å.

completion of the solvation shell of the charged guanidinium groups. A recent steered MD simulation of KvAP in an apolar octane layer found that hydrated chloride ions accompanied S4 arginines into the octane layer (34), which was not seen in our simulation. The likely explanation is that there is no physical necessity for chlorides to accompany the arginines into the hydrocarbon region, because salt bridges form between the arginine guanidiniums and lipid phosphates. Salt-bridge formation is entirely consistent with *ab initio* calculations by Green (35) that demonstrate strong complex formation between the guanidinium groups in the peptide LRIVRL and either HPO_4^{2-} or $H_2PO_4^-$. The sequence LRIVRL is a subsequence of a S4 segment.

The solvation shells of the charged guanidinium groups are dynamic, because of the thermal motion of the bilayer. The interactions defining these shells break and reform, leading to exchange of water molecules and phosphate groups. To quantify the lifetime of water molecules in the guanidinium solvation shells, a survival function (36) giving the average number of waters present in a particular solvation shell at a given time was computed (see *Supporting Text*, which is published as supporting information on the PNAS web site). Mean residence times were calculated as the corresponding average time constants obtained from stretched exponential fits to the survival functions. For comparison, the corresponding bulk water quantities were computed by performing the same analysis on water molecules 40 Å

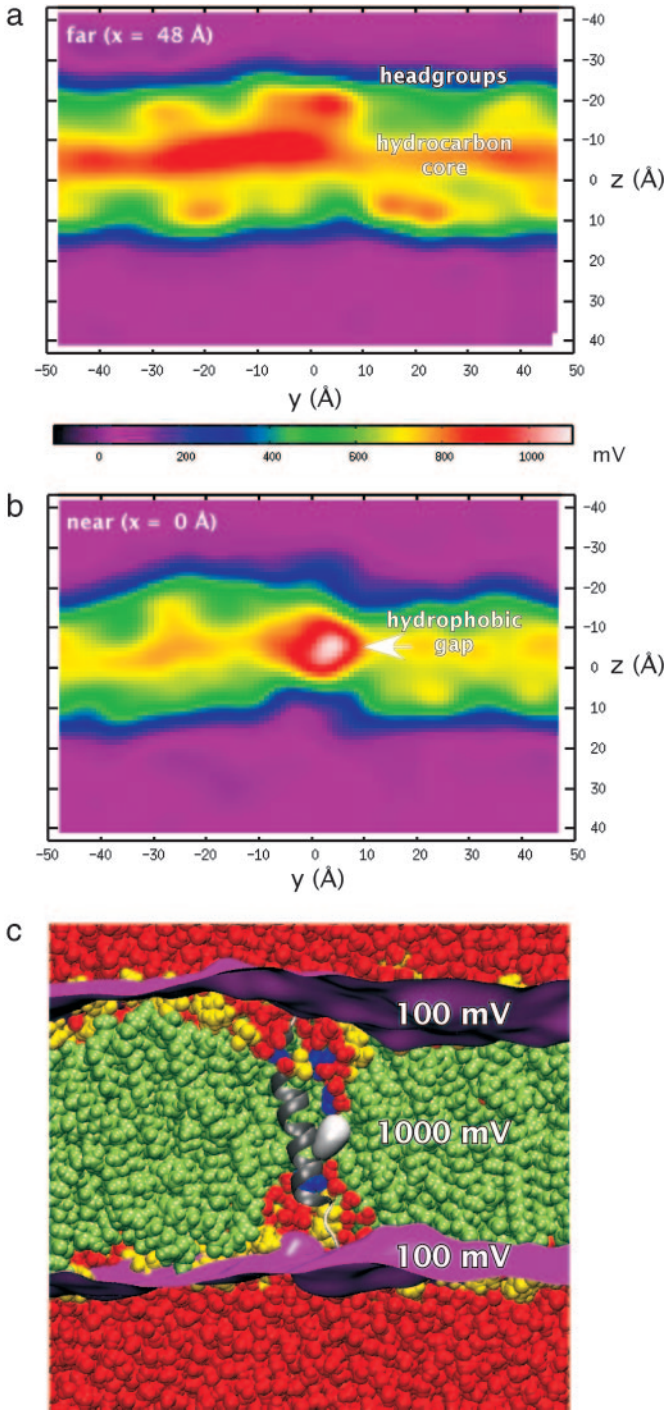

Fig. 4. Electrostatic potential distributions obtained by averaging 800 configurations spanning the last 8 ns of the simulation. The zero of potential is taken as the water. (*a*) Density map for the electrostatic potential distribution distant from the peptide (48 Å). The spatial distribution is characteristic of thermally disordered lipid bilayers, with relatively uniform contributions from the hydrocarbon core (red, yellow, green) and hydrated headgroup (blue) regions. The constant potential of the water map is shown in purple (see scale between *a* and *b*). (see also Fig. 5 and Movie 2) (*b*) Electrostatic potential distribution in a region centered on the peptide. The largest values of electrostatic potential (>1,000 mV) for the system are observed over a highly circumscribed region near the bilayer center (white). (*c*) 3D representations of two iso-potential surfaces are included in a space-filling representation similar to Fig. 1, confirming that the highest values of electrostatic potential occur in the vicinity of Arg-15 and Arg-18. The white surface (1,000 mV) surrounds the hydrophobic gap between these two residues. The purple surface (100 mV) shows the potential near the outer edge of the bilayer.

away from the center of mass of the peptide along the TM direction.

The survival functions plotted in Fig. 2*c* and the mean residence times listed in the legend demonstrate that water molecules remain in the hydrophilic neighborhoods for times orders of magnitude larger than in the same volume of bulk water phase. The faster dynamics for water molecules in the Arg-12 guanidinium coordination shell compared with the other guanidiniums is consistent with the observation that there is a single hydrophilic neighborhood for the guanidinium groups of Arg-9, Arg-12, and Arg-15, with the first coordination shell of Arg-12 side chain highly overlapping those of Arg-9 and Arg-15. The slower dynamics for water molecules in the coordination shell of Arg-15 and Arg-18 seems consistent with a local increase of the electric field, as explained below. The survival function calculated by taking into account the overlap of coordination shells for Arg-9, Arg-12, and Arg-15 to form a single hydrophilic neighborhood, indicated in Fig. 2*c* by the black curve, is remarkably similar to the survival function for Arg-18, consistent with the existence of two similar, but independent, solvation environments.

A visual inspection of the equilibrated trajectory showed that there were only two occurrences of guanidinium group exchange interactions with lipid phosphate groups during the last 8 ns of the simulation (see also Fig. 2*b* and Movie 1, which is published as supporting information on the PNAS web site). The two exchanging phosphate groups were observed to be interacting with more than one guanidinium group at a given time. Consequently, a more convenient characterization of the mobility of the guanidinium–phosphate complex is a comparison of the mean-square displacement (MSD) of the phosphate groups participating in the hydrophilic neighborhood with those at least 40 Å away from the peptide center of mass. The corresponding MSD values on the 1-ns time scale are 11 $Å^2$ for phosphate groups in the bulk lipid bilayer and 5 $Å^2$ for the phosphate groups in the first coordination shell of the guanidinium groups. Thus, both phosphate groups and water molecules are much less mobile in the vicinity of guanidinium groups than in their corresponding bulk environments.

The hydrophilic neighborhoods, seen most clearly in Fig. 3*a*, are separated by a nonpolar gap of ≈10 Å between Arg-15 and Arg-18. The gap was measured as the minimum distance between any water oxygen or phosphate atoms in the hydration shell of Arg-15 and Arg-18. No water molecules were observed to cross the gap by this measure or by visual inspection of the simulation trajectory. The gap was stable throughout the simulation (Fig. 3*b*), meaning that the effective dielectric thickness of the bilayer in the vicinity of S4 was much smaller than the typical bilayer hydrocarbon-core thickness (37) of 30 Å. Not surprisingly, this gap and the penetration of solvated Arg into the hydrocarbon core strongly perturb bilayer electrostatics (Fig. 4).

A 3D electrostatic potential map inside the bilayer was obtained from an average of a particle mesh Ewald calculation over 800 configurations, spanning the last 8 ns of the simulation (see *Methods* and Movie 2, which is published as supporting information on the PNAS web site). Fig. 4 shows two 2D slices through the bilayer (parallel to the bilayer normal), one 48 Å from the peptide (Fig. 4*a*) and the other centered on the peptide (Fig. 4*b*). The high thermal disorder of the bilayer is evident in the figures (see also Movie 2 and Fig. 5, which is published as supporting information on the PNAS web site). Relative to water, potentials inside the bilayer are positive, reaching values of ≈1 V that are typical of zwitterionic lipid bilayers (38, 39). The potential distribution in regions distant from the peptide (Fig. 4*a*) is generally symmetrical with respect to the bilayer midplane, arising mainly from contributions from the polarization of the terminal methyl/near-end methylene groups and hydrated headgroups. A localized, steep transition is observed across the bilayer interface, which is the thermally noisy atomistic version of the continuum description of the lipid bilayer as a parallel-plate capacitor. The electrostatic situation in the vicinity of the S4 peptide is dramatically different. The strong effect of the peptide on the bilayer electrostatic potential distribution is revealed by Fig. 4*b*. The S4 helix produces an irregular, diffuse profile throughout the bilayer interface region. The largest values of electrostatic potential of the entire system are found in a small region surrounding the hydrophobic gap (Fig. 4 *b* and *c*), indicative of a highly focused high-strength electric field around the hydrophobic gap. This is an expected consequence of the small effective thickness of the bilayer hydrocarbon core region in the vicinity of the peptide.

The results of the simulation show that charged amino acids can be stabilized in the membrane hydrocarbon core by aqueous solvation and the formation of salt bridges with lipid phosphate groups. How is this accomplished? Contrary to its depiction in continuum electrostatic models (17) as a homogeneous hydrocarbon slab with bulk properties, the lipid bilayer is composed of flexible amphiphilic molecules in a thermally disordered state (37). This flexibility apparently permits lipids in the immediate vicinity of the S4 peptide to adopt conformations that place their headgroups in contact with buried peptide charges, thereby providing a scaffold for water penetration. In a sense, the bilayer serves as a structural extension of the protein to enable a specific conformation, which may emerge as a general concept in membrane protein structural biology.

The traditional view of voltage sensing is that the S4 segment is surrounded by other protein TM domains. These form aqueous vestibules (canaliculi) that converge to a nonpolar region of <10 Å, across which the electric field is focused (3). Our simulation of S4 suggests a similar view, but one that does not involve the participation of other protein elements. This work offers a starting point for reconciling the traditional view of voltage sensing with the voltage paddle model, which locates the lipid-exposed S4 domain at the lipid–protein interface (10).

We thank Michael Myers for editorial assistance. This work was supported by grants from the National Institute of General Medical Sciences and the National Center for Research Resources (to S.H.W.); the National Science Foundation (to D.J.T.); and the Swedish Cancer Foundation, the Swedish Research Council, and the Marianne and Marcus Wallenberg Foundation (to G.v.H.). J.A.F. is supported by a National Research Service award from the National Library of Medicine.

1. Hille, B. (2001) *Ion Channels of Excitable Membranes* (Sinauer, Sunderland, MA).
2. Anderson, P. A. V. & Greenberg, R. M. (2001) *Comp. Biochem. Physiol. B* **129,** 17–28.
3. Bezanilla, F. (2000) *Physiol. Rev.* **80,** 555–592.
4. Cohen, B. E., Grabe, M. & Jan, L. Y. (2003) *Neuron* **39,** 395–400.
5. Miller, G. (2003) *Science* **300,** 2020–2022.
6. Starace, D. M. & Bezanilla, F. (2004) *Nature* **427,** 548–553.
7. Blaustein, R. O. & Miller, C. (2004) *Nature* **427,** 499–500.
8. Ahern, C. A. & Horn, R. (2004) *Trends Neurosci.* **27,** 303–307.
9. Jiang, Y. X., Ruta, V., Chen, J. Y., Lee, A. & MacKinnon, R. (2003) *Nature* **423,** 42–48.
10. Jiang, Y. X., Lee, A., Chen, J. Y., Ruta, V., Cadene, M., Chait, B. T. & MacKinnon, R. (2003) *Nature* **423,** 33–41.
11. Ruta, V., Jiang, Y. X., Lee, A., Chen, J. Y. & MacKinnon, R. (2003) *Nature* **422,** 180–185.
12. Long, S. B., Campbell, E. B. & MacKinnon, R. (2005) *Science* **309,** 897–903.
13. Long, S. B., Campbell, E. B. & MacKinnon, R. (2005) *Science* **309,** 903–908.
14. Goldstein, S. A. N. (1996) *Neuron* **16,** 717–722.
15. Halsall, A. & Dempsey, C. E. (1999) *J. Mol. Biol.* **293,** 901–915.
16. Mattila, K., Kinder, R. & Bechinger, B. (1999) *Biophys. J.* **77,** 2102–2113.
17. Parsegian, A. (1969) *Nature* **221,** 844–846.
18. Grabe, M., Lecar, H., Jan, Y. N. & Jan, L. Y. (2004) *Proc. Natl. Acad. Sci. USA* **101,** 17640–17645.
19. Hessa, T., White, S. H. & von Heijne, G. (2005) *Science* **307,** 1427.
20. Hessa, T., Kim, H., Bihlmaier, K., Lundin, C., Boekel, J., Andersson, H., Nilsson, I. M., White, S. H. & von Heijne, G. (2005) *Nature* **433,** 377–381.

21. Brooks, B. R., Bruccoleri, R. E., Olafson, B. D., States, D. J., Swaminathan, S. & Karplus, M. (1983) *J. Comput. Chem.* **4,** 187–217.
22. Kalé, L., Skeel, R., Bhandarkar, M., Brunner, R., Gursoy, A., Krawetz, N., Phillips, J., Shinozaki, A., Varadarajan, K. & Schulten, K. (1999) *J. Comput. Phys.* **151,** 283–312.
23. MacKerell, A. D., Jr., Bashford, D., Bellott, M., Dunbrack, R. L., Jr., Evanseck, J. D., Field, M. J., Fischer, S., Gao, J., Guo, H., Ha, S. *et al.* (1998) *J. Phys. Chem. B* **102,** 3586–3616.
24. Feller, S. E. & MacKerell, A. D., Jr. (2000) *J. Phys. Chem. B* **104,** 7510–7515.
25. Jorgensen, W. L., Chandrasekhar, J., Madura, J. D., Impey, R. W. & Klein, M. L. (1983) *J. Chem. Phys.* **79,** 926–935.
26. Essmann, U., Perera, L., Berkowitz, M. L., Darden, T., Lee, H. & Pedersen, L. G. (1995) *J. Chem. Phys.* **103,** 8577–8593.
27. Batcho, P. F., Case, D. A. & Schlick, T. (2001) *J. Chem. Phys.* **115,** 4003–4018.
28. Tuckerman, M. & Berne, B. J. (1992) *J. Chem. Phys.* **97,** 1990–2001.
29. Martyna, G. J., Tobias, D. J. & Klein, M. L. (1994) *J. Chem. Phys.* **101,** 4177–4189.
30. Feller, S. E., Zhang, Y., Pastor, R. W. & Brooks, B. R. (1995) *J. Chem. Phys.* **103,** 4613–4621.
31. Humphrey, W., Dalke, W. & Schulten, K. (1996) *J. Mol. Graphics* **14,** 33–38.
32. Harold, F. M. & Van Brunt, J. (1977) *Science* **197,** 372–373.
33. Dwyer, J. J., Gittis, A. G., Karp, D. A., Lattman, E. E., Spencer, D. S., Stites, W. E. & García-Moreno, E. B. (2000) *Biophys. J.* **79,** 1610–1620.
34. Monticelli, L., Robertson, K. M., MacCallum, J. L. & Tieleman, D. P. (2004) *FEBS Lett.* **564,** 325–332.
35. Green, M. E. (2005) *J. Theor. Biol.* **233,** 337–341.
36. Impey, R. W., Madden, P. A. & McDonald, I. R. (1983) *J. Phys. Chem.* **87,** 5071–5083.
37. Wiener, M. C. & White, S. H. (1992) *Biophys. J.* **61,** 434–447.
38. Tobias, D. J., Tu, K. & Klein, M. L. (1997) *Curr. Opin. Colloid Interface Sci.* **2,** 15–26.
39. Tobias, D. J. (2001) *Curr. Opin. Struct. Biol.* **11,** 253–261.